inter.noise
HAMBURG 2016

Numerical Simulation of a Benchmark Case for Aerodynamics and Aeroacoustics of a Low Pressure Axial Fan

Clemens Junger[1]; Florian Zenger[2]; Aaron REPPENHAGEN[3];
Manfred KALTENBACHER[4]; Stefan BECKER[5]

[1,4] TU Wien, Austria

[2,5] Friedrich-Alexander University Erlangen-Nuremberg, Germany

[3] Virtual Vehicle, Austria

ABSTRACT

A benchmark case for aerodynamics and aeroacoustics of a low pressure axial fan was investigated numerically. The aerodynamic simulations were computed with ANSYS Fluent and OpenFOAM. The aeroacoustic source terms and wave propagation were computed in the time domain with the multiphysics research software CFS++, using the perturbed convective wave equation. The computed aerodynamic and aeroacoustic results were compared with measurement data. Thereby, a good agreement could be achieved. However, the accuracy of the numerical simulations strongly depends on the mesh resolution and computed real time.

Keywords: Axial fan, Benchmark, FEM I-INCE Classification of Subjects Numbers: 11.4.1, 75.3

1. INTRODUCTION

Nowadays numerical prediction of fan characteristics requires not only aerodynamic but also aeroacoustic computations. Thereby, numerical simulations are often difficult to validate, especially if there are no experimental results available. Therefore, benchmark cases are needed to evaluate the reliability of numerical simulations. Gained experience can then be transferred to similar applications where no experiments exist and measurement data cannot be obtained. The computation of rotating geometries makes the numerical methods even more complex and special benchmarks are needed to yield additional information, for example about non conforming interfaces. Carolus et al. provided a benchmark of a fan in a long duct (1). Zanon et al. provided an open rotor and compared measurement results with computational fluid dynamics (CFD) and computational aeroacoustic (CAA) results gained from the Ffowcs Williams-Hawkings (FWH) analogy (2).

In this work we want to investigate the benchmark of Zenger et al., which provides measurement data of a fan in a short duct (3). The fan geometry is easy to reproduce, because NACA profiles were used for the blade geometry and it was already subject to further investigations in (4) and (5). In contrast to the work of Zanon, we don't use the integral FWH method to compute the acoustics but use a volume discretization of the acoustic domain, where a transient acoustic wave propagation is computed. This method was already successfully applied in (6) and (7).

First, a brief overview of the benchmark case is given (for details see (3,4)). Second, the acoustic analogy is explained before the CFD and CAA setups are discussed. Finally, the obtained CFD and CAA results are compared with the measurements.

2. MEASUREMENTS

The experimental investigations were done at the Institute of Process Machinery and Systems

[1] clemens.junger@tuwien.ac.at
[2] ze@ipat.uni-erlangen.de
[3] aaron.reppenhagen@v2c2.at
[4] manfred.kaltenbacher@tuwien.ac.at
[5] sb@ipat.uni-erlangen.de

Engineering (iPAT) at the Friedrich-Alexander University of Erlangen-Nuremberg. The measurements were made in an standardized inlet test chamber, with anechoic walls. The volumetric flow was adjusted by butterfly dampers and an auxiliary fan, and was rectified in the inlet chamber. The fan duct was installed in the wall of the inlet chamber, with the suction side to the chamber and the pressure side facing outwards. The fan itself was driven by an electric motor outside the test chamber. The main fan parameters are shown in Table 1.

Table 1 – Fan design parameters

Fan diameter	495mm
Tip clearance	2.5mm
Hub diameter	248mm
Duct length	390mm
Rounds per minute	1486min^{-1}
Max. tip velocity	38.9m/s
Number of blades	9
Blade passing frequency	225Hz
Max. Re number	$1.5 \cdot 10^5$
Volumetric flow	1.4m^3/s
Pressure difference	150Pa

The maximum tip velocity corresponds to a Mach number smaller than 0.12, thus the flow can be considered incompressible in the numerical simulation; the Reynolds number indicates a turbulent flow, hence a turbulence model has to be used in the numerical simulation.

3. THEORY

The numerical method used in this work is based on a forward coupling between a flow simulation and an acoustic propagation simulation. The flow simulation is solved with a finite volume flow solver. The flow results are used to compute acoustic source terms as a right hand side for an acoustic analogy. The acoustic source terms are interpolated on a (generally) coarser acoustic mesh to safe computational effort (8). The partial differential equation of the acoustic analogy, that describes the sound propagation, is then solved with our finite element multi-physics software CFS++ (9).

The aeroacoustic analogy used in this paper is based on the acoustic perturbation equations (APE-2) for incompressible flow derived by Ewert (10). In these equations, the flow quantities are split under the assumption of a mean field with small alternating amplitudes (perturbations). The ansatz decomposes the fluid velocity $\mathbf{u}$ in a mean velocity field $\bar{\mathbf{u}}$ and the alternating quantities in a purely incompressible part $\mathbf{u}^{\mathrm{ic}}$ and a purely acoustical part $\mathbf{u}^{\mathrm{a}}$. This decomposition is also done for the pressure p as shown in eq. (1).

$$\mathbf{u} = \bar{\mathbf{u}} + \mathbf{u}^{\mathrm{ic}} + \mathbf{u}^{\mathrm{a}};\ p = \bar{p} + p^{\mathrm{ic}} + p^{\mathrm{a}} \tag{1}$$

This set of APE-2 was adapted for low Mach numbers and isothermal flow by Hüppe (11) and reduced to a single perturbed convective wave equation (PCWE)

$$\frac{\mathrm{D}^2\varphi^{\mathrm{a}}}{\mathrm{D}t^2} - \nabla \cdot \nabla\varphi^{\mathrm{a}} = -\frac{1}{\rho c_o^2}\frac{\mathrm{D}p^{\mathrm{ic}}}{\mathrm{Dt}} \ . \tag{2}$$

In (2) ρ denotes the density, c_0 the speed of sound and φ^{a} the acoustic scalar potential. The acoustic scalar potential computes as

$$\mathbf{u}^{\mathrm{a}} = -\nabla\varphi^{\mathrm{a}}. \tag{3}$$

The acoustic source term on the right hand side of eq. (2) is just dependent on the substantial derivative of the incompressible pressure, since ρ and c_0 were assumed to be constant. The partial derivative for a stationary domain is

$$\frac{\mathrm{D}}{\mathrm{D}t} = \frac{\partial}{\partial t} + \bar{\mathbf{u}} \cdot \nabla. \tag{4}$$

For a rotating domain, as it was used for this fan, the mean velocity has to be corrected by the rotational velocity $\mathbf{u}_\mathrm{r}$ and the partial derivative becomes

$$\frac{\mathrm{D}}{\mathrm{D}t} = \frac{\partial}{\partial t} + (\bar{\mathbf{u}} - \mathbf{u}_\mathrm{r}) \cdot \nabla. \tag{5}$$

The acoustic pressure can be easily obtained from the acoustic potential by

$$p^\mathrm{a} = \rho \frac{\mathrm{D}}{\mathrm{D}t} \varphi^\mathrm{a}. \tag{6}$$

Note that the mean flow in the partial derivative of eq. (4) and (5) implies a steady state of the flow, so for example a run up of a fan cannot be simulated.

4. SIMULATION

Two CFD simulations were performed on the same mesh, one with ANSYS Fluent and another one with the open source program OpenFOAM. The mesh consists of about 19 million hexadominant cells, without structured wall layers. The whole mesh was divided into three main regions, as shown in Figure 1. The inlet chamber on the left and the outlet area on the right are stationary. The fan region, in between both stationary regions, is rotating. Nonconforming interfaces are used to connect the stationary and rotating regions. The motor was simplified to a uniform shaft and a cylindrical body, to account for the blockage in the outflow.

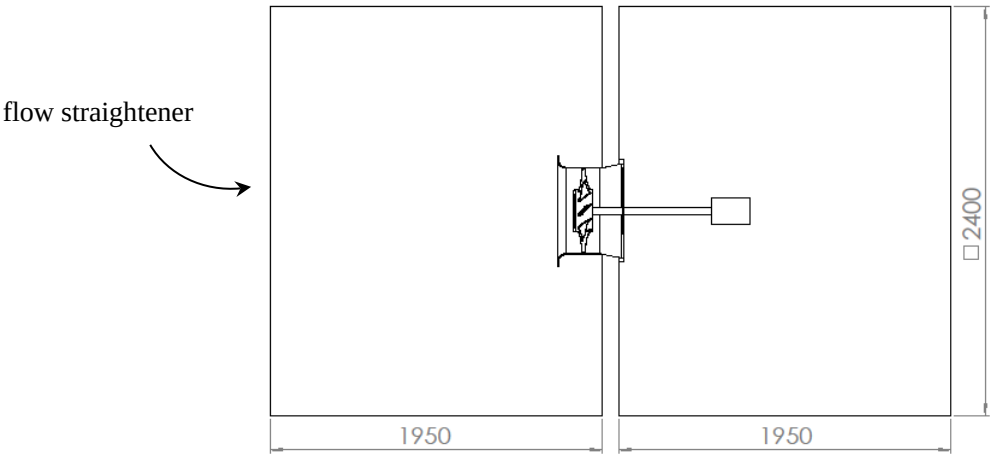

Figure 1 – Geometry of the simulation domain

The inlet domain has the same cross section as the measurement facility and begins shortly after the flow rectifier of the test chamber. The rectified flow is represented in the simulation by a uniform velocity inlet. All other walls in the inlet chamber are treated with no slip boundary conditions. The outlet domain was chosen with the same volume as the inlet domain. To represent the free outflow from the test facility to atmosphere, the outer boundaries are set to pressure outlet. The wall between inlet and outlet region, as well as the whole rotor geometry are treated with no slip boundary conditions.

The used turbulence model is in both simulations a detached eddy simulation (DES) to account for the required modeling of small turbulence structures. The time step size is set to $\Delta t = 10\mu s$. In the case of the Fluent simulation five revolutions of the rotor are computed to reach a steady state and export of flow data is started. In the case of OpenFOAM 15 revolutions are computed before the export. The total export time is 0.13s which is equivalent to 3.2 revolutions. In Fluent the acoustic source term of eq. (2) is computed and stored on run time, whereas in OpenFOAM the flow quantities are stored and the source term is computed as a post-process.

The acoustic mesh also consists of two stationary and one rotating domains (see Figure 2). The rotating CAA domain (red) has the same size as the rotating CFD domain and is also connected to the

stationary domains with nonconforming interfaces. The inlet and outlet domain (blue) are reduced in size, to decrease computational effort, where the outlet domain is cropped so that the most important source terms in the free stream are still included. The inlet domain is the main propagation domain of the simulation and its size is chosen to include all microphone positions of the measurement. The mesh size is generated with a maximum spacing of 23.5mm to resolve frequencies up to f=1500Hz with at least 10 elements per wavelength. The total number of mesh nodes is about 2.3 million. The time step size in the CAA simulation is $\Delta t = 20\mu s$. To account for the anechoic conditions in the inlet chamber and the free field radiation of the free outflow a perfectly matched layer (green) is used in CFS++.

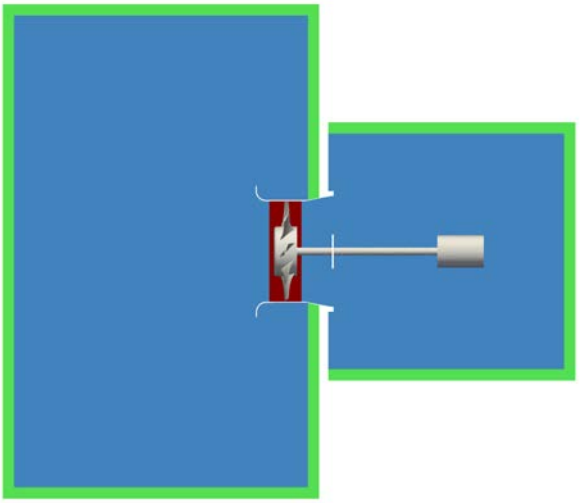

Figure 2 – Acoustic mesh zones

5. RESULTS

In this section, results from the measurements and the numerical simulations are compared at the design volumetric flow of 1.4m^3/s of the fan as shown in Table 1. It includes results from the aerodynamics and acoustics of the fan.

5.1 Flow Results

One main characteristic of a fan is the pressure difference between suction and pressure side. The pressure difference is obtained in a region without significant influence of the fan. The results are shown in Table 2.

Table 2 – Pressure in the chamber

	Measurement	Fluent	OpenFOAM
p (Pa)	126.5	114.4	124.0

The measurement shows that the design pressure difference is not exactly reached, because several effects were neglected in the design process, like losses in the hub region, influence of the backflow in the tip region and the installation of the fan in a relatively short duct. The deviation between the measurement and the simulations is 9.6% in the case of Fluent and 2.0% in the case of OpenFOAM.

Figure 3 shows the averaged axial velocity between the hub and the duct, on the suction and pressure side. The simulated values are in the same range as the measured ones, but local deviations occur on the suction and pressure side. The Fluent simulation overestimates the velocity in the outer region but finally underestimates the velocity at the tip region. On the pressure side the velocity is underestimated in the outer region. Maybe the deviations near the walls result from the wall function in the turbulence model and a mesh refinement should be considered in further simulations.

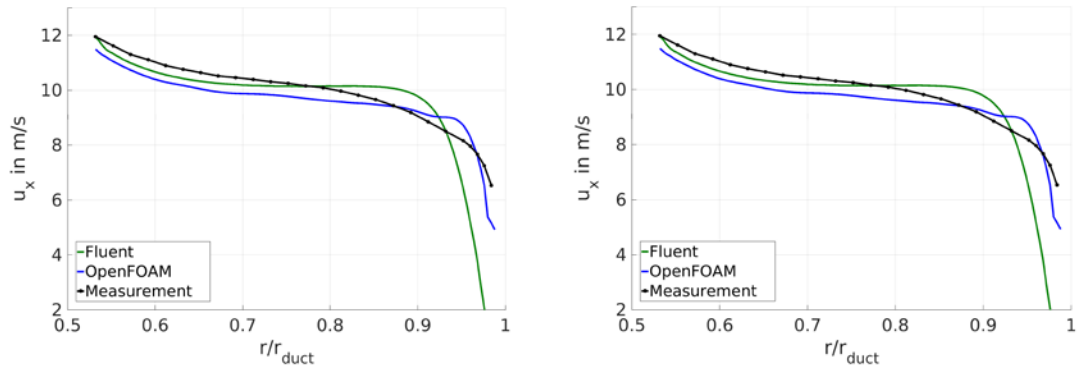

(a) suction side (b) pressure side

Figure 3 – Time averaged axial velocity

The wall pressure fluctuations were measured in the duct at 15 probe locations, equally distributed with a spacing of 10mm, with the first probe 15mm behind the intersection of the inlet nozzle and the straight duct. The power spectral density (PSD) of the wall pressure fluctuations of four different probes are shown in Figure 4.

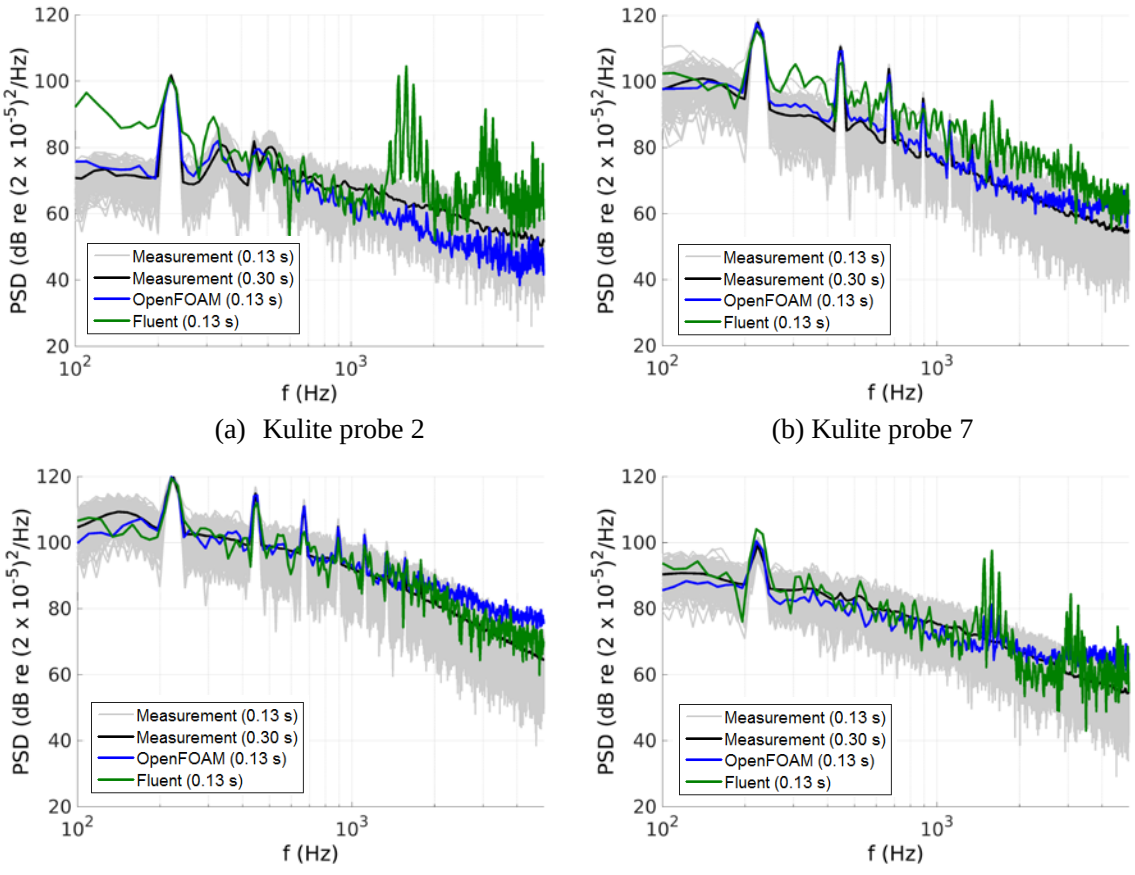

(a) Kulite probe 2 (b) Kulite probe 7

(c) Kulite probe 8 (d) Kulite probe 14

Figure 4 – Pressure probes in the duct

The measurement is shown as the black line and the grey line represents the measurement data split in batches of equivalent time to the simulated results. In the Fluent simulation unphysical peaks occur around 1500Hz at probe 2 and 14, which might result from the close distance to the nonmatching interfaces. Due to the fact that we use the flow result for acoustic computations, designed for frequencies up to 1500Hz, this seems to be negligible. Probe 2 (Figure 4a) is before the blades, on the

suction side of the fan, close to the nonmatching interface between the inlet chamber and the rotating domain. Probes 7 and 8 (Figure 4b and 4c) are in the middle of the rotating region where the blade tips are passing and probe 14 (Figure 4d) is behind the blades on the suction side, close to the nonmatching interface between the rotating domain and the outlet domain. Both simulations are able to estimate the peak at the blade passing frequency of 225Hz very well. The subharmonic peak at 335Hz is overestimated by Fluent in Figure 4a. In Figure 4b the higher harmonics of the blade passing frequency are reproduced by both solvers, but the broad band fluctuations are overestimated by Fluent. In Figure 4d the blade passing frequency is overestimated by Fluent whereas the broad band fluctuations are underestimated by OpenFOAM.

5.2 Acoustic Results

The acoustic measurement was done with 7 microphones in a half circle, with 1m radius, in front of the duct inlet. The power spectral density of probe 1 (perpendicular to the nozzle) to 4 (directly in front of the duct) is shown in Figure 5.

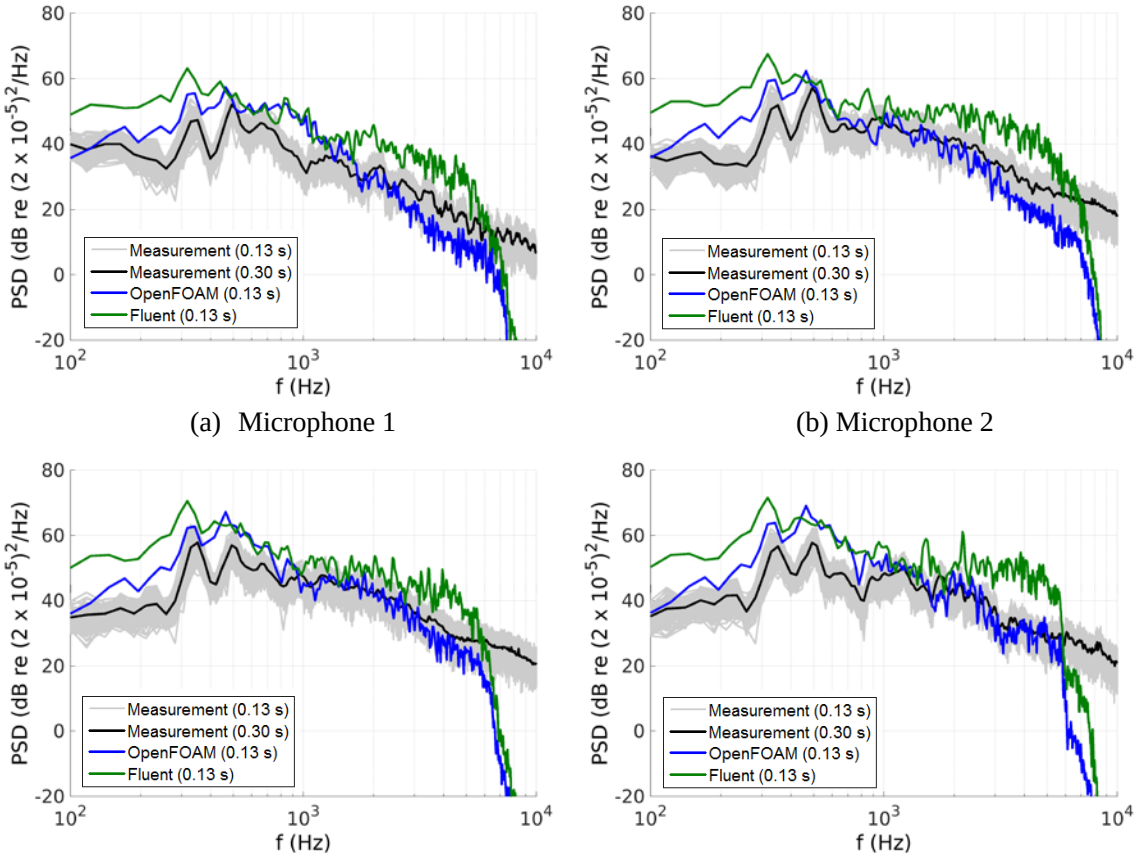

(a) Microphone 1 (b) Microphone 2

(c) Microphone 3 (d) Microphone 4

Figure 5 – PSD of the acoustic signal

Above the mesh design frequency of 1500Hz the results from the Fluent simulation overestimate the PSD and the results from the OpenFOAM simulation underestimate the PSD. Above 5kHz the results of both simulations drop drastically when the spatial resolution of the grid becomes too coarse, to resolve the acoustic wavelength. Overall the acoustic PSD of the simulation with source terms from Fluent is higher than from the OpenFOAM simulation, but both simulations reproduce the characteristic subharmonic peak at around 335Hz. The results from the OpenFOAM simulation fit the measurements better in the lower frequencies but in the mid frequency range both databases are similar. In Figure 5a the amplitude is overestimated between 800Hz to 1200Hz and for the probes more in front of the duct the over estimation shifts to lower frequencies (in Figure 5dto 400Hz to 800Hz). In the very low frequencies, the simulation time (and therefore the signal length) was not long enough to give a detailed resolution.

6. CONCLUSION

The rotor benchmark as published in (3) was reproduced numerically and aerodynamic and acoustic quantities were compared between measurements and simulations. The CFD results of Fluent and OpenFOAM were in good agreement with the measurements. Since the same mesh was used for both simulations, the differences in the numerical solutions may result from the different flow initialization time and/or the solver parameters itself. The acoustic pressure obtained with the database of Fluent tend to overestimate the PSD in lower and higher frequencies, but in the mid frequency range both databases have a similar PSD. An improvement in the numerical treatment of this benchmark could be made by the resolution of the CFD database, which would include mesh refinement especially in the wall regions and a longer real time of the simulation. Furthermore, the acoustic result could be improved by a grid refinement to resolve higher frequencies. Further investigations of this benchmark are planned.

ACKNOWLEDGEMENTS

The computational results presented have been achieved using the Vienna Scientific Cluster (VSC).

REFERENCES

1. T. Carolus, T. Zhu, and M. Sturm. A low pressure axial fan for benchmarking prediction methods for aerodynamic performance and sound. Proceedings of the International Conference on Fan Noise, Technology and Numerical Methods; Lyon, France 2015.
2 A. Zanon, M. De Gennaro, H. Kuehnelt, and D. Caridi. Broadband noise of axial fans: an experimental and computational benchmark study. In 19th AIAA/CEAS Aeroacoustic Conference; Berlin, Germany 2013.
3 F. Zenger, C. Junger, M. Kaltenbacher, and S. Becker. A Benchmark Case for Aerodynamics and Aeroacoustics of a Low Pressure Axial Fan. SAE Technical Paper 2016-01-1805, 2016.
4 F. Zenger, M. Becher, and S. Becker. Influence of inflow turbulence on aeroacoustic noise of low speed axial fans with skewed and unskewed blades. Proceedings of the International Conference on Fan Noise, Technology and Numerical Methods; Lyon, France 2015.
5 F. Zenger and S. Becker. Einfluss der Zuströmbedingungen auf die aeroakustische Schallabstrahlung von gesichelten und ungesichelten Axialventilatoren. In 41. Jahrestagung für Akustik, DAGA; Nürnberg, Germany 2015. p. 422–425
6 A. Hüppe, M. Kaltenbacher, A. Reppenhagen, F. Zenger, S. Becker, and K. Habr. Computational aeroacoustics for ducted fans. In The 22nd International Congress on Sound and Vibration; Florence, Italy 2015.
7 M. Kaltenbacher, A. Hüppe, A. Reppenhagen, M.Tautz, S.Becker, and W.Kuehnel. Computational aeroacoustics for hvac systems utilizing a hybrid approach. SAE International,9(3), May 2016. 2016-01-1808.
8 A. Hüppe and M. Kaltenbacher. Investigation of interpolation strategies for hybrid schemes in computational aeroacoustics. In 41. Jahrestagung für Akustik, DAGA; Nürnberg, Germany 2015. p. 872–875
9 M. Kaltenbacher. Numerical Simulation of Mechatronic Sensors and Actuators. Springer, Berlin Germany, 3. edition, 2015.
10 R. Ewert and W. Schröder. Acoustic perturbation equations based on flow decomposition via source filtering. Journal of Computational Physics, 188:365–398, 2003.
11 A. Hüppe, J. Grabingery, M. Kaltenbacher, A. Reppenhagen, and W. Kühnel. A non-conforming finite element method for computational aeroacoustics in rotating systems. In American Institute of Aeronautics and Astronautics Conference; San Diego, USA 2014.